3D Printable Sensorized Soft Gelatin Hydrogel for Multi-Material Soft Structures

David Hardman, Josie Hughes, Thomas George Thuruthel, Kieran Gilday, and Fumiya Iida, *Senior Member, IEEE*

***Abstract*—The ability to 3D print soft materials with integrated strain sensors enables significant flexibility for the design and fabrication of soft robots. Hydrogels provide an interesting alternative to traditional soft robot materials, allowing for more varied fabrication techniques. In this work, we investigate the 3D printing of a gelatin-glycerol hydrogel, where transglutaminase is used to catalyse the crosslinking of the hydrogel such that its material properties can be controlled for 3D printing. By including electron-conductive elements (aqueous carbon black) in the hydrogel we can create highly flexible and linear soft strain sensors. We present a first investigation into adapting a desktop 3D printer and optimizing its control parameters to fabricate sensorized 2D and 3D structures which can undergo >300% strain and show a response to strain which is highly linear and synchronous. To demonstrate the capabilities of this material and fabrication approach, we produce some example 2D and 3D structures and show their sensing capabilities.**

***Index Terms*—Robot sensing systems, soft robotics, three-dimensional printing.**

I. Introduction

THE development of new materials and fabrication techniques is fundamental to the construction of soft robots [1], [2]. Many soft robots are currently fabricated from elastomeric materials such as silicones, which allow for complex, homogeneous, and highly flexible structures [3]. Whilst these have attractive properties for many applications, the use of such materials often limits the fabrication process to casting. In addition, the inclusion of soft sensors in this process can be challenging, and often the resultant sensor properties are sub-optimal due to poor interfacing between the elastomer and the conductive particle [4]. There has been exploration of a variety of approaches for 3D printing soft structures and robots with embedded sensors, including direct 3D printing [5], embedded 3D printing [6] or multi-nozzle printing [7]. However, despite the many advances that have been seen, it is still a challenge to develop low-cost techniques that can fabricate truly soft and homogeneous structures with robust embedded sensing capabilities. The incorporation of conductive filaments into flexible actuators has yielded promising sensor responses [8], though durability and ductility limitations can hinder their soft robot applications.

Hydrogels are an interesting alternative to traditional materials for the fabrication of soft robots. They are particularly appealing because of the vast range and variety of mechanical properties that can be achieved with relative ease [9]. There has been prior investigation into the fabrication of hydrogels for soft robots [10], [11], with the highly extensible properties showing promise [12]. There has been exploration of generating strain sensors using hydrogels [13], [14], and recent works have demonstrated methods to print conductive hydrogels to fabricate strain sensors [15]–[17]. Their high water content offers potentially favourable sensor properties over inorganic alternatives [18]. However, fabrication techniques are constrained to specialized bioprinters and UV-cured materials. The goal of this work is to explore methods of 3D printing soft hydrogel structures with embedded resistive sensors using widely available modified desktop 3D printers,materials that are cheap and easy to obtain, and requiring no additional apparatus for curing.

We propose a method of fabricating soft, sensorized structures using a hydrogel based on gelatin and glycerol. By adding appropriate amounts of the enzyme transglutaminase to the hydrogel, crosslinking is triggered which starts gelation and enables control of the material properties for 3D printing. By optimizing the composition of the hydrogel, we ensure the material is both printable and has elastomeric-like performance, making it suitable for soft robotic applications. A modified desktop 3D printer can then be used for additive manufacturing. In addition, we show that conductive carbon black particles can be dispersed in the hydrogel to create an organic strain sensitive material. Due to increased homogeneity and biocompatibility, suitable mechanical properties, and higher compatibility between the conductive fillers and crosslinked polymer networks, hydrogels appear to be a better alternative to traditional silicone-based sensing technologies [19]. We employ a novel approach of using carbon black to form electron-conductive hydrogels that have higher gauge factor and higher robustness than ion-conductive hydrogels, exhibiting excellent synchronicity between the mechanical and electrical signal and good stability under repeated load. Similar findings have been reported for carbon nanotube based conductive hydrogels [20]. Moreover, our designs are biodegradable, translucent, cheap and involve no hazardous chemicals or materials throughout the fabrication process.

Manuscript received October 23, 2020; accepted February 23, 2021. Date of publication April 12, 2021; date of current version April 29, 2021. This letter was recommended for publication by Associate Editor R. MacCurdy and Editor K.-J. Cho upon evaluation of the reviewers' comments. This work was supported in part by SHERO project, a Future and Emerging Technologies (FET) programme of the European Commission Grant Agreement ID 828818, and in part by EPSRC DTP EP/R513180/1. *(David Hardman and Josie Hughes contributed equally to this work.) (Corresponding author: David Hardman.)*

The authors are with the Department of Engineering, Bio-Inspired Robotics Lab, University of Cambridge, Cambridge CB3 9ET, U.K (e-mail: dsh46@cam.ac.uk; jaeh2@cam.ac.uk; tg444@cam.ac.uk; jaeh2@cam.ac.uk; fi224@cam.ac.uk).

This letter has supplementary downloadable material available at https://doi.org/10.1109/LRA.2021.3072600, provided by the authors.

Digital Object Identifier 10.1109/LRA.2021.3072600

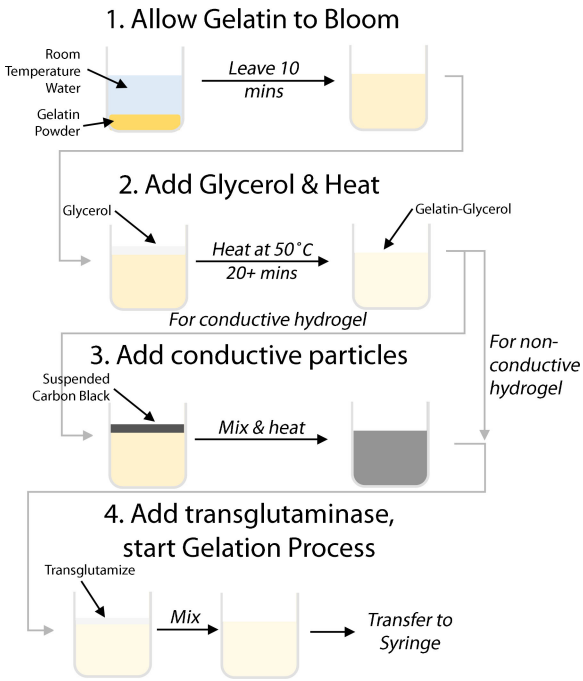

Fig. 1. Flow chart summarizing the process of preparing the gelatin based hydrogel from the different components.

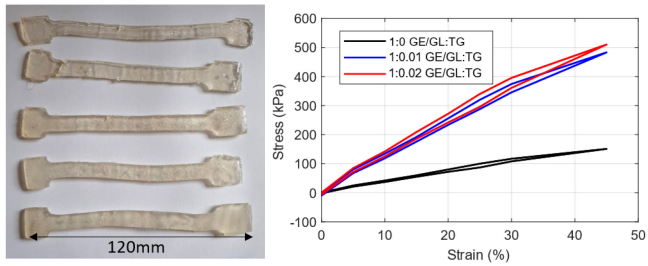

Fig. 2. Cast dog-bone samples created for stress-strain tests (left). Average stress-strain curves for 3 example samples (right). The strain was increased at a rate of 50 mm/second, and the cycles were repeated 30 times.

In this letter we provide the method for fabricating the hydrogel material and the conductive hydrogel sensors, highlighting that it is easy and low cost to fabricate and uses widely available 'food safe' materials. We show how this material can undergo >300% strain, and how the sensor properties show a high sensitivity and high linearity compared to a number of existing sensorized hydrogels, making the material extremely promising for soft robotic applications. To show how the fabrication can be customized and automated, we demonstrate how the crosslinking can be controlled for 3D printing using an enzyme. We demonstrate the 3D printing of hydrogel sensors, and the fabrication of multi-material sensorized structures with transversely isotropic layers. By designing the insulating and conductive layers to have similar material properties, the elongations of multi-material structures are not constrained by the embedded sensors, and we avoid morphological distortions caused by interfacial stresses. This work serves as a first demonstration of the material and fabrication approach, though there is significant room for future optimization of both.

In the following section of this letter we introduce the method by which the hydrogel is created, and its material properties. We also demonstrate the capabilities of the sensorized hydrogel, highlighting the high gauge factor, linearity and low drift. In Section III we focus on the experimental setup enabling 3D printing of the hydrogels. In the Results section we demonstrate the printing capabilities for 2D and 3D structures. Finally, we discuss the limitations and future direction in Section V.

II. Methods

A. Hydrogel Preparation

The hydrogel is prepared from a mix of gelatin (GE), glycerol (GL) and the enzyme transglutaminase (TG); the process is summarized in Fig. 1. Gelatin hydrogels have been widely explored for uses in in pharmaceutical and medical applications due to their biocompatibility and biodegradability [21], [22]. They have also been explored for the 3D printing of edible and self healing structures [22], [23].

To prepare the hydrogel, cold water is first added to the powdered gelatin and the mix is allowed to bloom. Glycerol is then added to the mix to increase the bound-water content of the hydrogel. The mix is placed in a water bath at 50 degrees Celsius. Based on previous exploration [24], [25], the ratio of the components is chosen to be 1:1.5:8 by mass for gelatin, glycerol and water respectively.

To prepare the sensorized gelatin hydrogel (SGH), aqueous carbon black (CB) is added to the mix and allowed to homogenise. The addition of conductive elements to hydrogels and specific gelatin-based hydrogels has been explored previously [26]–[28], and is a widely used approach for developing inorganic strain and pressure sensors [29]–[31].

Transglutaminase (TG), otherwise known as 'meat glue,' is an enzyme that catalyses the crosslinking of the gelatin chains [32]. The use of TG removes the needs for toxic crosslinkers and bypasses undesired side reactions due to the specificity of the enzymes. It allows for rapid crosslinking, converting the liquid GE/GL mix into an extrudable gel.

B. Hydrogel Properties

To explore the material properties, a number of dogbone shaped samples with various GE/GL:TG ratios were cast and allowed to crosslink for 12 hours. These samples were cyclically strain tested, with the load measured. The results and samples are shown in Fig. 2. In all cases the curve is approximately linear with little hysteresis. In the samples to which the crosslink-inducing TG has not been added, the material has a lower stiffness. In the crosslinked samples, the incorporation of increasing amounts of TG does not seem to affect the final Young's moduli (Table I).

To measure the maximum tensile strain, increasing strain was applied to the sample until fracture. These results are summarized in Table I, with two representative samples shown in Fig. 3. It can be seen the addition of TG significantly increases the maximum strain that can be achieved from 240% to over 300%.

TG also affects the working 'pot life,' defined as the time after TG's addition that the mixture is an extrudable gel. Fig. 4 shows how the material properties of the mix vary with time after the TG is added. Using this, it is possible to tune the GE/GL:TG ratio

TABLE I
MATERIAL PROPERTIES FOR MATERIAL SAMPLES DEVELOPED WITH VARYING RATIOS OF GE/GL:TG. SHOWS THE YOUNG'S MODULUS, MAXIMUM STRAIN THAT CAN BE REACHED AND THE USABLE POT LIFE

Ratio	Youngs Modulus (kPa)	Max Strain (%)	Pot Life (mins)
1:0	3.3	235	-
1:0.005	10.6	240	10
1:0.01	10.8	285	8
1:0.015	10.7	290	6
1:0.02	10.8	320	4

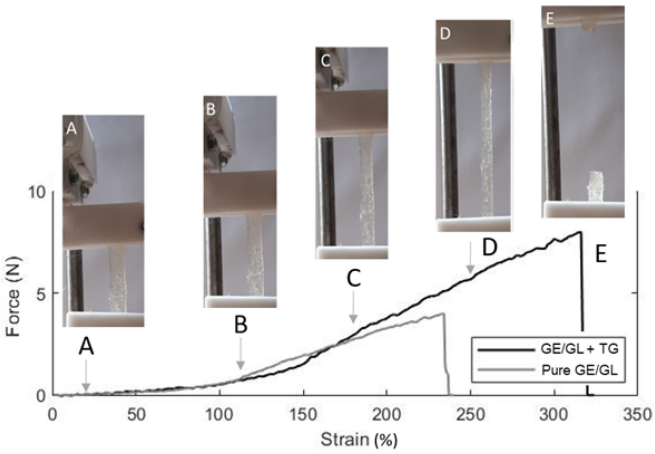

Fig. 3. Tensile strength tests, with the strain applied increased until failure. Accompanying pictures show the sample undergoing increasing strain.

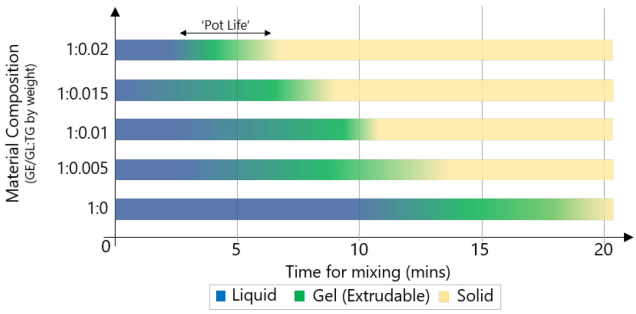

Fig. 4. The variation in material properties after TG's addition for various GE/GL:TG ratios, showing the progression from liquid to gel and solid, and demonstrating that the pot life can be tuned using the amount of enzyme added.

to optimize the pot life for 3D printing. The gel's temporal properties are adapted to each print: small samples can be fabricated and crosslinked without delay using high TG concentrations, whilst the longer pot life at lower concentrations provides a consistent viscosity throughout a longer print.

C. Sensorized Hydrogels

By adding aqueous conductive particles - in this case a carbon black ink - to the GE/GL mix, the hydrogel can be made conductive and strain sensitive. To demonstrate the properties of this sensorized hydrogel (SHG) a number of dog-bone shaped samples have been cast using various ratios of CB ink. The

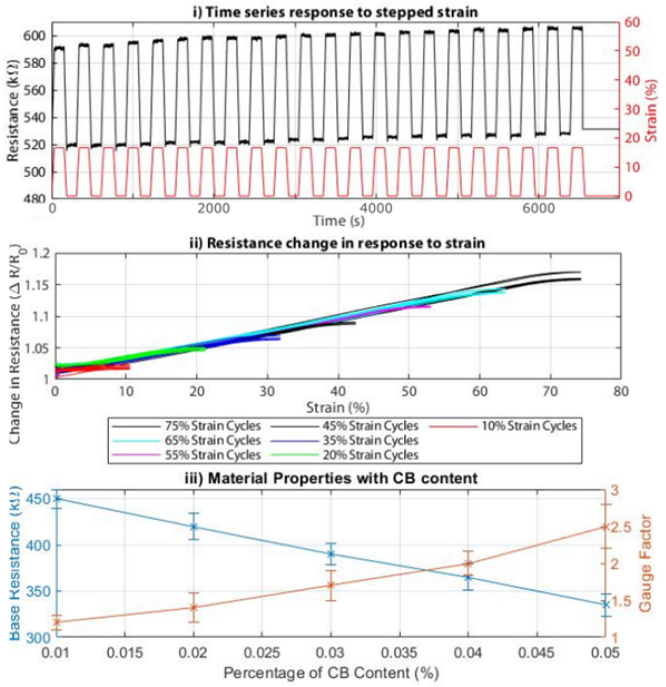

Fig. 5. Characterization of the SHG sensor (0.03% CB content). i) Time series response to a cyclic step and hold strain, ii) Resistance change in response to applied cyclic strains of various magnitude as denoted by the legend. iii) Variation of material properties in response to varying percentage of CB inclusion by weight.

sensor response has been characterized by capturing the resistance across the sensor when various strain profiles are applied using a custom made material testing device. The resistance is measured using an Arduino microcontroller with a 10-bit ADC. An example time series response to a cyclic step and hold strain pattern is shown in Fig. 5 i. The sensor shows a fast response to the applied strain: the phase delay is found to be 21 ms, though this could be limited by the 50 Hz sampling rate. The average overshoot is just 2.9% of the step magnitude, with a maximum of 6.4% during the release of the third strain cycle. The drift is also low, with the steady state maxima and minima increasing by an average of 0.9% & 0.6% of the step magnitude per cycle, respectively. To test the linearity, strain cycles of various magnitude have been applied to the sensor, and the resistance measured. The results are shown in Fig. 5 ii. The response is highly linear, with little hysteresis.

To investigate the effect of CB concentration on the sensor properties, varying amounts of CB were incorporated in the hydrogel and the strain properties measured. In particular, the base resistance and the dimensionless gauge factor $((\frac{\Delta R}{R})/\varepsilon)$ were measured. Fig. 5 iii shows that the gauge factor increases with the ratio of CB ink included in the mix. The dilution caused by higher CB ratios is detrimental to the material properties: the Young's modulus decreases, and failure occurs at lower strains.

To quantify the performance of the sensor in comparison to others, we have computed a number of metrics, namely the linearity, phase lag and gauge factor. These are presented in Table II, where a limited comparison is to made to a selection of other sensorized hydrogels. Whilst this table is not an exhaustive

TABLE II
TABLE SUMMARIZING THE PROPERTIES OF THE SGH IN COMPARISON TO NUMBER OF EXISTING HYDROGEL BASED SENSORS

Sensorized Hydrogel	Sensor Type (Strain/Pressure)	Gauge Factor	Linearity (R^2 Value)	Maximum Strain	3D Printability	Material Toxicity	Sensing Characteristics
K-carrageenan/PAAm [33]	S (Resistive)	0.63	-	1400%	Bioprinting (Ink Printing)	High	-Low Drift -Some Non-linearities
DMA/SDS/NaCl (NaCl nanoparticles) [16]	S, P (Capacitative)	1	-	200%	Ink Extrusion	Medium	-Approx. linear -Temp. Stability
Gelatin & Tannic Acid [23]	S (Resistive)	< 1	-	1500%	No	Low	-Self Powered
PAA/nano barium ferrite [34]	S (Resistive)	1-3	-	100%	No	Some	-Low hysteresis
CNT/Borax/PVA [13]	S (Resistive)	1.51	-	1000%	No	Medium	- Self Healing
Stick on Sensors [35]	S (Resistive)	2-3	0.9745	400%	No	Low	- High repeatability
Cellulose Ionic hydrogels [36]	S (Resistive)	0.3	0.963	126%	No	Organic	- Temp. stability
SGH (This work)	**S +P (Resistive)**	**2.5**	**0.9887**	**320%**	Extrusion Based	**-Low Cost -Food Safe**	**-High Linearity -Low Drift**

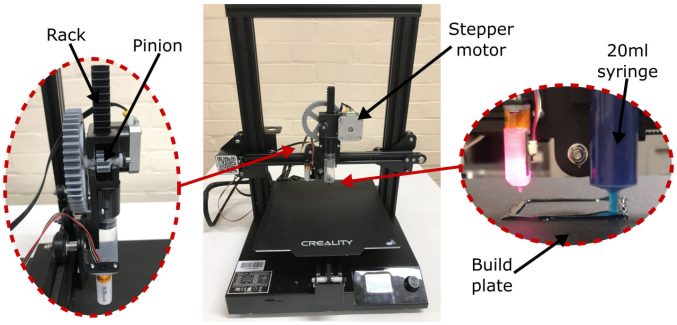

Fig. 6. The modified desktop printer. The usual thermoplastic extrusion apparatus is replaced by a liquid deposition mechanism, controlled by a stepper motor.

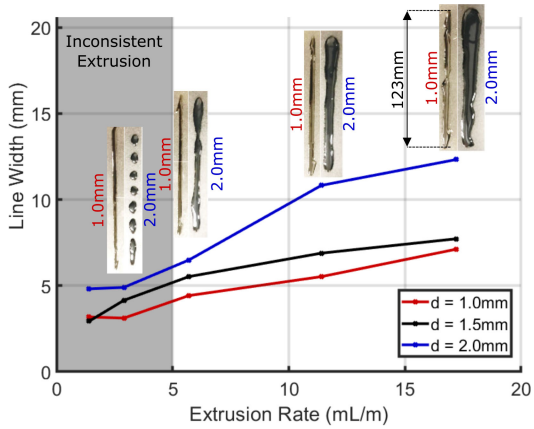

Fig. 7. Variation of printed line width with extrusion rate and nozzle diameter. Examples of $d = 1$ mm and $d = 2$ mm lines are given, each with length 123 mm. Below 5 mL/m, extrusion was inconsistent, often depositing droplets rather than a single line.

comparison, it highlights the advantages of this approach in that it shows a high linearity, is non-toxic, 3D printable, and has a good gauge factor. Although further work is required to fully characterize the sensor performance, the results show promise in comparison to existing alternatives.

III. 3D PRINTING EXPERIMENTAL SETUP

Once the hydrogel's extrudable pot life has been optimized, its extrusion from a syringe forms the basis of the simple printing mechanism. A modified *Creality CR-20* desktop FDM printer (Fig. 6) is controlled using a PC running *Pronterface* via USB. The hot end and cooling fans are replaced by a custom hydrogel deposition mechanism, fabricated from 62 g of printed PLA, 6 M3 screws, and a 5 mm steel axle. The printer's original stepper motor controls the plunger of a 20 ml syringe using a rack and pinion, with 15 mm pinion pitch diameter. A gear ratio of 1:5, 1.8° step angle, and 16× microstepping correspond to 339.5 microsteps per mm of linear plunger motion, or 1181 microsteps per mL of extruded material. The GE/GL mix is sucked into the syringe by immersing the nozzle and slowly reversing the extrusion mechanism.

The line width during printing is dependant on a range of factors, including the extrusion rate, nozzle diameter, and hydrogel rheology. The latter is influenced by the hydrogel composition, quantity of transglutaminase, and the printing window after TG addition, which are held constant at 1:1.5:8 GE:GL:H_2 O, 1:0.007 GE/GL:TG, and 5-9 minutes respectively. With the nozzle size kept constant, the effects of extrusion rate and nozzle size on the line width are explored via a set of single line calibration tests, using digital calipers to measure the width of the crosslinked lines in 3 locations. The line printing order is varied during the 4 repetitions over which each test is averaged, minimizing any effects of progressive gelation. Once this data has been gathered, the nozzle diameter d is changed and the process repeated: the results are plotted in Fig. 7.

Regardless of nozzle diameter, too low an extrusion rate did not reliably deposit a steady stream of material on the build plate, and is denoted by the 'Inconsistent Extrusion' region in Fig. 7. We select a rate of 5.7 mL/m and a $d = 2$ mm nozzle diameter for subsequent tests, giving a continuous line of printed material. Whilst finer resolutions are achieved with smaller d, the wider choice eliminates dangers of nozzle clogging, but is still capable of printing a range of geometries.

Fig. 7's line widths are also dependent on the mixture's properties. Since the lines contain the same volume of material at a given extrusion rate, differences in width are accompanied by changes in height, requiring a sufficient viscosity for their stability. As such, we expect lower viscosities to result in increased line widths, enabling tuning of the print properties through the GE:GL:H_2 O & GE/GL:TG ratios. Provided the nozzle was low enough to adhere a steady stream of substrate to

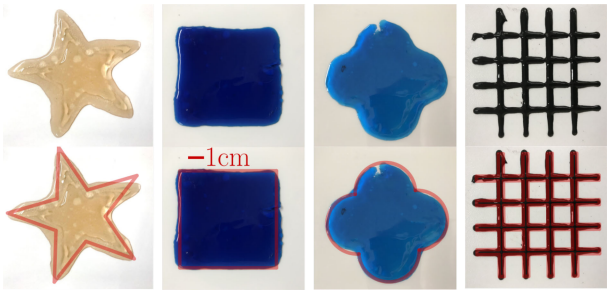

Fig. 8. Examples of printed 2D hydrogel structures. The top row shows the printed shape, the bottom overlays the input shape.

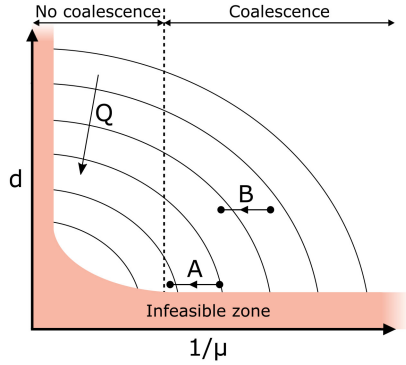

Fig. 9. A model demonstrating the effects of nozzle diameter d and hydrogel viscosity μ on print quality Q. Contours of constant Q are marked.

the build plate without flattening, small deviations in height were found to have little effect on the line width. Using these control parameters, simple 2D outlines are printed directly from G-code, whilst filled shapes are created using a customised *Cura* profile. The relatively low viscosity caused by these parameters during the pot life allows adjacent lines to coalesce into a transversely isotropic continuous shape, with planar properties independent of the printing direction. Gentle manipulations of the print (such as removal from the build plate) are possible approximately 5 minutes after the pot life ended; the samples are left for a further 12 hours for crosslinking to complete.

Basic 3D structures are created by layering successive prints, leaving a short period for crosslinking. In Section IV-C's examples, each layer is loaded individually to the printer. The nozzle is cleared between layers to prevent crosslinked hydrogel from creating an airtight stopper. The setup is designed such that the syringe can easily be removed to accommodate this cleaning.

IV. Results

A. Printing Demonstration

To demonstrate the printing capabilities, a variety of hydrogel structures have been produced. We first present a number of 2D structures (Fig 8), printed as a single layer using the hydrogel composition and $d = 2$ mm nozzle size chosen during the preliminary experiments. The structures are colored using food dye, and the desired input shape is overlaid onto Fig. 8.

We see that the macroscopic shapes are all fabricated to a recognisable standard, though resolution tends to be lost at sharp corners. Two major factors are capable of causing this effect: the 2 mm nozzle diameter, and the 'pooling' of low viscosity gels after printing. Fig. 9 suggests a qualitative model of their effects on print resolution/quality Q when other control parameters are held constant. The 'infeasible zone' encompasses combinations of diameter d and viscosity μ for which printing is not possible, due to physical system constraints and setup limitations such as motor torque. Contours of constant Q are marked; better resolution is expected as d decreases and as μ increases, retaining sharp corners. By ignoring thixotropic behaviors and assuming coalescence to be independent of d, we suggest a μ threshold at which coalescence between neighbouring lines becomes possible. This simplification incorporates the interplay between viscosity and surface tension, often represented in inkjet printing using the dimensionless Ohnesorge number [37].

To obtain transversely isotropic layers, we wish coalescence to occur throughout printing. Since the hydrogel becomes increasingly viscous over its pot life, path A indicates the optimum strategy for maximising Q: at the end of its pot life, the hydrogel lies at the boundaries of coalescence and infeasibility. In practice, these boundaries are not strictly defined: partial coalescence is possible, and the infeasibility zone represents the parameters for which printing is *most likely* to fail. Our experiments operated far from these boundaries (path B) to maximise the likelihood of successful coalescence. Further improvement in print quality Q is therefore possible: careful control of d and μ would enable fabrication to occur at their Pareto front.

Additionally, it is noted that Fig. 8's images show the structures after removal from the base plate. Some apparent distortions - such as the deviated angle of a star's arm - are likely due to the hydrogel's flexibility, and are not reflections of printing errors.

B. Printed Sensors

To demonstrate the printing of hydrogel sensors and the flexibility in morphology this offers, we have fabricated a set of sensors with varying morphology, as shown in Fig. 10. To investigate the different responses we strain cycle the sensors. Electrodes are connected to the ends of the sensor and the resistance measured using a microcontroller. The sensor responses are shown in Fig. 10. We believe some of the drift seen in the sensor responses may result from slight slipping in the mechanical testing device, By exploiting 3D printing to control the morphology, sensors displaying specific response behaviors can be designed and fabricated. Here we briefly show how the cross-sectional area affects the stress-strain behavior (gradient); being able to control the sensor morphology via 3D printing enables more complex optimization of sensor morphologies [38].

C. 3D Printed Multi-Material Sensorized Structures

By layering successive prints, combinations of conductive and insulating cross sections allow the fabrication of sensorized structures. To demonstrate this method, we first consider a simple multi-layer bending sensor (Fig. 11), fabricated from two layers of conductive hydrogel separated by an insulating layer. Fig. 11 shows the sensor's response to linear stretching and single-axis bending. Both sensorized layers respond equally to

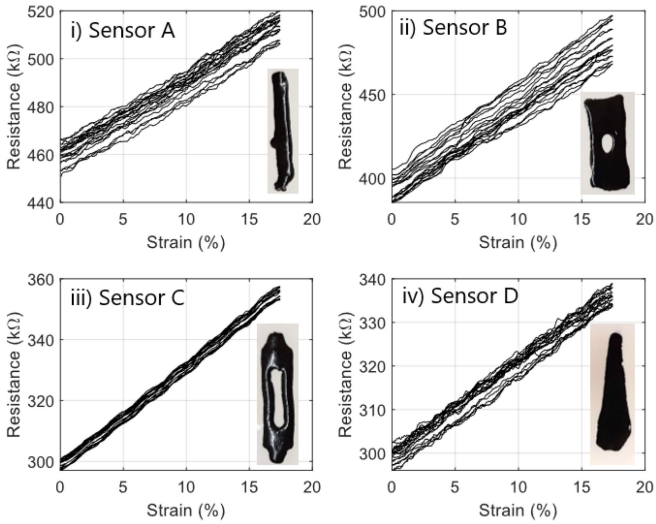

Fig. 10. Examples of various morphology 3D printed sensors, and their resistive sensor responses to cyclic strain, repeated 20 times for each sensor.

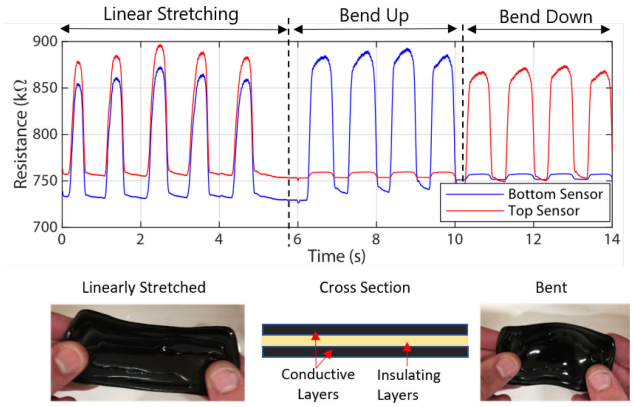

Fig. 11. Demonstration of a three layer (conductive, insulating, conductive) bending sensor (below). Time series plot showing the sensor's response to manual stretching and bending (above).

the linear strain, whereas during bending the layer under tension shows the greatest change in resistance. The responses from both tests are noise free and repeatable, demonstrating not only how multiple layers can be embedded into a soft structure, but also the potential of this method in the fabrication of sensorized 3D soft robotic components.

Finally, we present an actuated and sensorized 3D multi-material finger (Fig. 12), consisting of 6 printed hydrogel layers: C–I–I–I–I–C,, where C & I denote conductive and insulating layers, respectively. The sensorized bottom layer enables proprioceptive sensing, whilst the finger 'pads' provide feedback from environmental interactions. Tubular sections were manually added after the completion of the second layer, which became embedded in the finger. The fully printed structure was left to crosslink overnight before a tendon was threaded through the tube, providing a simple method of bending actuation via control of the tendon's tension.

To test the embedded proprioceptive sensor, cyclic bending tests were performed, controlled using the tendon. By connecting electrodes to the two ends of the layer, the sensor response

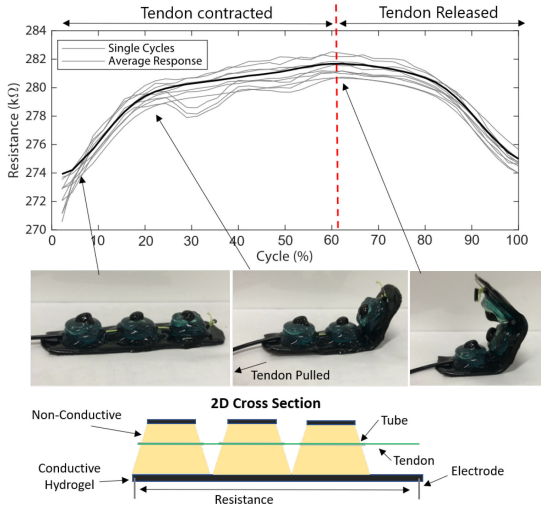

Fig. 12. A 3D printed multi-material structure with embedded sensor, with the sensor response shown for repeated cyclic bending.

could be measured with a microcontroller. This experiment was repeated, with the repeated cycles and average response during the bending cycle shown in Fig. 12. The resistance increases until the finger is fully bent, and decreases when the tendon is released. The results show a repeatability between cycles and a significant change in resistance with bending-induced strain. The differences in behavior between cycles is believed to result from the physical bending behavior of the finger.

These demonstrations serve as an initial demonstration of the capabilities of this fabrication approach, and provide some exploration of their application to robotics and sensing applications.

V. DISCUSSION & CONCLUSION

In this letter we have proposed a method of 3D printing gelatin/glycerol hydrogels. We introduce non-sensorized and sensorized hydrogels which can be 3D printed to fabricate soft structures which can undergo 300% strain. Through the dispersion of carbon black in the hydrogel, we obtain conductive materials that have superior sensing properties compared to silicone-based sensors, but are easy to develop and print with respect to other hydrogel-based sensors. Using this approach, we demonstrate the printing of a number of sensorized 2D and 3D structures which show great promise in their sensor linearities, low drift and rapid responses. This work provides a first demonstration of this approach, and validates the use of hydrogels for the low cost fabrication of soft robots with embedded soft strain sensors.

With the current setup, the size of each layer is limited by the syringe volume. This is straightforward to extend, provided a suitably timed pot life is selected. If the syringe is re-filled between each layer, the vertical height is bounded only by the build volume & the print's stability. Though repeated refilling is labour intensive in the preliminary setup, automation offers a route to improvement.

As is often seen in additive manufacturing, the structures' properties perpendicular to the build plate are influenced by weaker interfaces between its layers. Investigations into these

interfacial strengths would benefit further investigations into tuning the material properties for printing. However, the transversely isotropic layers produced by the hydrogel's coalescence offer improved uniformity over traditional extrusion techniques.

There is significant scope for future development of this initial exploration. Fig. 9 proposes three available methods of improving print quality in future work: reducing the nozzle size whilst avoiding the infeasible zone; increasing the hydrogel's final viscosity whilst maintaining coalescence, and minimising the range of viscosity over the extrudable pot life. Material properties can be tuned by introducing additional controls: temperature dependence shows promise for further investigations, as does the automated mixing of GE/GL and TG in the extruder to provide a longer pot life. The manufacture of hydrogel composites deserves further research: combining our liquid deposition mechanism with an FDM hot end would enable the manufacture of sensorized skeletal structures, support materials for internal cavities, and thermoplastic elastomer integration. Unlike silicone alternatives, the hydrogel's low melting point can be exploited during this process: localised melting of the area surrounding the FDM nozzle could be used to create airtight interfaces between materials, or to embed solid inclusions into the hydrogel print. With these improvements the application domain can be explored to show increasingly complex 3D sensorized structures for soft robotics and wearable applications.

References

[1] F. Iida and C. Laschi, "Soft robotics: Challenges and perspectives," *Procedia Comput. Sci.*, vol. 7, pp. 99–102, 2011.

[2] F. Ilievski, A. D. Mazzeo, R. F. Shepherd, X. Chen, and G. M. Whitesides, "Soft robotics for chemists," *Angewandte Chemie*, vol. 123, no. 8, pp. 1930–1935, 2011.

[3] C. Majidi, "Soft-matter engineering for soft robotics," *Adv. Mater. Technol.*, vol. 4, no. 2, 2019, Art. no. 1800477.

[4] M. Amjadi, K.-U. Kyung, I. Park, and M. Sitti, "Stretchable, skin-mountable, and wearable strain sensors and their potential applications: A review," *Adv. Funct. Mater.*, vol. 26, no. 11, pp. 1678–1698, 2016.

[5] O. D. Yirmibesoglu *et al.*, "Direct 3 d printing of silicone elastomer soft robots and their performance comparison with molded counterparts," in *Proc. IEEE Int. Conf. Soft Robot.*, 2018, pp. 295–302.

[6] R. L. Truby *et al.*, "Soft somatosensitive actuators via embedded 3D printing," *Adv. Mater.*, vol. 30, no. 15, 2018, Art. no. 1706383.

[7] M. A. Skylar-Scott, J. Mueller, C. W. Visser, and J. A. Lewis, "Voxelated soft matter via multimaterial multinozzle 3D printing," *Nature*, vol. 575, no. 7782, pp. 330–335, 2019.

[8] T. Hainsworth, L. Smith, S. Alexander, and R. MacCurdy, "A fabrication free, 3d printed, multi-material, self-sensing soft actuator," *IEEE Robot. Automat. Lett.*, vol. 5, no. 3, pp. 4118–4125, Jul. 2020.

[9] M. Oyen, "Mechanical characterisation of hydrogel materials," *Int. Mater. Rev.*, vol. 59, no. 1, pp. 44–59, 2014.

[10] M. Baumgartner *et al.* "Resilient yet entirely degradable gelatin-based biogels for soft robots and electronics," *Nature Mater.*, pp. 1–8, 2020.

[11] H. Banerjee, M. Suhail, and H. Ren, "Hydrogel actuators and sensors for biomedical soft robots: Brief overview with impending challenges," *Biomimetics*, vol. 3, no. 3, 2018, Art. no. 15, doi: 10.3390/biomimetics3030015 .

[12] Y. Cheng *et al.*, "Direct-ink-write 3 d printing of hydrogels into biomimetic soft robots," *ACS Nano*, vol. 13, no. 11, pp. 13 176–13 184, 2019.

[13] G. Cai, J. Wang, K. Qian, J. Chen, S. Li, and P. S. Lee, "Extremely stretchable strain sensors based on conductive self-healing dynamic cross-links hydrogels for human-motion detection," *Adv. Sci.*, vol. 4, no. 2, 2017, Art. no. 1600190.

[14] Y.-J. Liu, W.-T. Cao, M.-G. Ma, and P. Wan, "Ultrasensitive wearable soft strain sensors of conductive, self-healing, and elastic hydrogels with synergistic "soft and hard" hybrid networks," *ACS Appl. Mater. Interfaces*, vol. 9, no. 30, pp. 25 559–25 570, 2017.

[15] S. Liu and L. Li, "Ultrastretchable and self-healing double-network hydrogel for 3 d printing and strain sensor," *ACS Appl. Mater. Interfaces*, vol. 9, no. 31, pp. 26 429–26 437, 2017.

[16] Z. Lei, Q. Wang, and P. Wu, "A multifunctional skin-like sensor based on a 3 d printed thermo-responsive hydrogel," *Mater. Horiz.*, vol. 4, no. 4, pp. 694–700, 2017.

[17] K. Tian *et al.*, "3 d printing of transparent and conductive heterogeneous hydrogel-elastomer systems," *Adv. Mater.*, vol. 29, no. 10, 2017, Art. no. 1604827.

[18] Y. Lee, W. Song, and J.-Y. Sun, "Hydrogel soft robotics," *Mater. Today Phys.*, vol. 15, 2020, Art. no. 100258.

[19] X. Sun, F. Yao, and J. Li, "Nanocomposite hydrogel-based strain and pressure sensors: A review," *J. Mater. Chem. A*, vol. 8, no. 36, pp. 18 605–18623, 2020.

[20] J. Huang, M. Zhao, Y. Cai, M. Zimniewska, D. Li, and Q. Wei, "A dual-mode wearable sensor based on bacterial cellulose reinforced hydrogels for highly sensitive strain/pressure sensing," *Adv. Electron. Mater.*, vol. 6, no. 1, 2020, Art. no. 1900934.

[21] S. Van Vlierberghe, P. Dubruel, and E. Schacht, "Biopolymer-based hydrogels as scaffolds for tissue engineering applications: A review," *Biomacromolecules*, vol. 12, no. 5, pp. 1387–1408, 2011.

[22] M. Stevenson, J. Long, P. Guerrero, K. de la Caba, A. Seyfoddin, and A. Etxabide, "Development and characterization of ribose-crosslinked gelatin products prepared by indirect 3D printing," *Food Hydrocolloids*, vol. 96, pp. 65–71, 2019.

[23] J. Wang, F. Tang, Y. Wang, Q. Lu, S. Liu, and L. Li, "Self-healing and highly stretchable gelatin hydrogel for self-powered strain sensor," *ACS Appl. Mater. Interfaces*, vol. 12, no. 1, pp. 1558–1566, 2019.

[24] J. Shintake, H. Sonar, E. Piskarev, J. Paik, and D. Floreano, "Soft pneumatic gelatin actuator for edible robotics," in *Proc. IEEE/RSJ Int. Conf. Intell. Robots Syst.*, 2017, pp. 6221–6226.

[25] J. Hughes and D. Rus, "Mechanically programmable, degradable & ingestible soft actuators," in *Proc. 3rd IEEE Int. Conf. Soft Robot.*, 2020, pp. 836–843.

[26] L. Han *et al.*, "Mussel-inspired adhesive and conductive hydrogel with long-lasting moisture and extreme temperature tolerance," *Adv. Funct. Mater.*, vol. 28, no. 3, 2018, Art. no. 1704195.

[27] P. He *et al.*, "Anti-freezing and moisturizing conductive hydrogels for strain sensing and moist-electric generation applications," *J. Mater. Chem. A*, vol. 8, no. 6, pp. 3109–3118, 2020.

[28] Z. Shao *et al.*, "Degradable self-adhesive epidermal sensors prepared from conductive nanocomposite hydrogel," *Nanoscale*, vol. 12, no. 36, pp. 18771–18781, 2020, doi: 10.1039/D0NR04666C.

[29] J. Hughes and F. Iida, "Localized differential sensing of soft deformable surfaces," in *Proc. IEEE Int. Conf. Robot. Automat.*, 2017, pp. 4959–4964.

[30] J. Hughes and F. Iida, "Tack and deformation based sensorised gripping using conductive hot melt adhesive," in *Proc. IEEE Int. Conf. Soft Robot.*, 2018, pp. 553–558.

[31] J. Hughes and F. Iida, "Tactile sensing applied to the universal gripper using conductive thermoplastic elastomer," *Soft Robotics*, vol. 5, no. 5, pp. 512–526, 2018.

[32] J. J. Y. Tan, C. P. Lee, and M. Hashimoto, "Preheating of gelatin improves its printability with transglutaminase in direct ink writing 3D printing," *Int. J. Bioprint.*, vol. 6, no. 4, 2020, Art. no. 296, doi: 10.18063/ijb.v6i4.296.

[33] S. Liu, Y. Qiu, W. Yu, and H. Zhang, "Highly stretchable and self-healing strain sensor based on gellan gum hybrid hydrogel for human motion monitoring," *ACS Appl. Polym. Mater.*, vol. 2, no. 3, pp. 1325–1334, 2020.

[34] H. Gu *et al.*, "Smart strain sensing organic-inorganic hybrid hydrogels with nano barium ferrite as the cross-linker," *J. Mater. Chem. C*, vol. 7, no. 8, pp. 2353–2360, 2019.

[35] S. Cheng, Y. S. Narang, C. Yang, Z. Suo, and R. D. Howe, "Stick-on large-strain sensors for soft robots," *Adv. Mater. Interfaces*, vol. 6, no. 20, 2019, Art. no. 1900985.

[36] R. Tong *et al.*, "Highly stretchable and compressible cellulose ionic hydrogels for flexible strain sensors," *Biomacromolecules*, vol. 20, no. 5, pp. 2096–2104, 2019.

[37] B. Derby, "Inkjet printing of functional and structural materials: Fluid property requirements, feature stability, and resolution," *Annu. Rev. Mater. Res.*, vol. 40, no. 1, pp. 395–414, 2010.

[38] T. G. Thuruthel, J. Hughes, and F. Iida, "Joint entropy-based morphology optimization of soft strain sensor networks for functional robustness," *IEEE Sensors J.*, vol. 20, no. 18, pp. 10 801–10810, 2020.